ADVANCES IN PHYSICS: X, 2017
VOL. 2, NO. 2, 281–301
http://dx.doi.org/10.1080/23746149.2017.1282834

Taylor & Francis
Taylor & Francis Group

REVIEW ARTICLE

OPEN ACCESS

The growth and degradation of binary and ternary octahedral Pt–Ni-based fuel cell catalyst nanoparticles studied using advanced transmission electron microscopy

Marc Heggen, Martin Gocyla and Rafal E. Dunin-Borkowski

Ernst Ruska-Centre for Microscopy and Spectroscopy with Electrons and Peter Grünberg Institute, Forschungszentrum Jülich GmbH, Jülich, Germany

ABSTRACT

Advances in fuel cell technology depend strongly on the development of affordable, active, and stable catalysts. For example, octahedral Pt–Ni alloy nanoparticles show exceptional activity for the oxygen reduction reaction in fuel cell cathodes as a result of the presence of highly active {1 1 1} facets. Here, we review a selection of recent transmission electron microscopy studies that address the correlation between the catalytic performance of octahedral Pt–Ni-based nanoparticles and their atomic-scale structure and composition. We begin by describing strategies for the growth of binary Pt–Ni and ternary Pt–Ni–TM (TM = transition metal) nanoparticles, with a focus on understanding how their structure and compositional anisotropy is related to their catalytic activity and stability. We then describe the morphological changes and compositional degradation effects that can occur in electrochemical environments. Changes in nanoparticle shape, including the loss of highly active {1 1 1} facets due to dealloying from Ni-rich facets and Pt surface diffusion, are discussed as important reasons for catalyst degradation. Finally, strategies to prevent degradation, e.g. by surface doping, are addressed. The growth, segregation, and degradation mechanisms that we describe highlight the complexity with which octahedral alloy nanoparticles form and evolve under reaction conditions.

ARTICLE HISTORY
Received 3 November 2016
Accepted 11 January 2017

KEYWORDS
Fuel cell catalysts; Transmission electron microscopy; Pt–Ni nanoparticles

PACS
Electron microscopy in structure determination, 68.37.Lp; high-resolution transmission electron microscopy (HRTEM), 68.37.Og; scanning transmission electron microscopy (STEM), 68.37.Ma; structure of Nanoparticles, 61.46.Df

1. Introduction

Developments in fuel cell technology are of great importance for energy conversion and storage applications. Proton-exchange membrane (PEM) fuel cells are attracting particular interest as clean power sources for mobile and stationary devices. However, a major obstacle that currently limits their performance

CONTACT Marc Heggen m.heggen@fz-juelich.de
© 2017 The Author(s). Published by Informa UK Limited, trading as Taylor & Francis Group.
This is an Open Access article distributed under the terms of the Creative Commons Attribution License (http://creativecommons.org/licenses/by/4.0/), which permits unrestricted use, distribution, and reproduction in any medium, provided the original work is properly cited.

is the sluggish oxygen reduction reaction (ORR) at fuel cell cathodes. Although Pt-based catalysts show very high activity and stability in PEM fuel cells [1,2], it is important to reduce the proportion of rare and expensive Pt that they contain without compromising their activity for the ORR, for example by alloying them with abundant low-cost transition metals [3–19]. Such alloying strategies can be used to introduce lattice compression effects [20,21] and/or modified electronic properties [22,23]. For instance, in 2010 Strasser et al. demonstrated that the Pt-rich shell in a bimetallic Cu–Pt core/shell nanoparticle exhibits compressive strain, resulting in a shift of the electronic band structure of Pt and weakening the chemisorption of oxygenated species [21].

In 2007, Stamenkovic et al. demonstrated that the Pt_3Ni (1 1 1) alloy surface has exceptionally high activity for the ORR [6]. They showed that it is 10 times more active than the Pt (1 1 1) surface and 90 times more active than state-of-the-art Pt/C catalysts. The Pt_3Ni (1 1 1) surface has an unusual electronic structure, which is related to the position of its d-band center [6]. Its near-surface layers were shown to exhibit a compositional oscillation, with Pt-rich outermost and third layers and a Ni-rich second layer. Such a surface Pt atomic layer is often referred to as a Pt skin [24–26]. The weak interaction between the Pt surface atoms and non-reactive oxygenated species increases the number of active sites for O_2 adsorption. As a consequence of the exceptionally high ORR activity of the Pt_3Ni (1 1 1) surface, (1 1 1)-faceted octahedral Pt–Ni nanoparticles have been considered the ultimate 'dream electrocatalysts' [27], with significant efforts dedicated to the synthesis of uniform octahedral Pt–Ni nanoparticles of controlled size and composition [7,9,28–32].

Here, we review recent transmission electron microscopy (TEM) studies of the growth of Pt–Ni-based nanoparticles, concentrating on the relationship between their structures, compositions, and catalytic properties, as well as their degradation in electrochemical environments and strategies that can be used to prevent such degradation.

2. Synthesis of octahedral Pt–Ni nanoparticles

Nanoparticles that take the form of octahedra, cubes, or truncated octahedra are, in general, terminated by {1 1 1} or {1 0 0} facets and are often synthesized by making use of capping agents that selectively control the growth rates of individual facets [33–36]. For example, in 2010 Zhang et al. described the successful synthesis of Pt_3Ni nanocubes and nanooctahedra and assessed the relationships between their activities and facets [7]. Unfortunately, however, the capping agents that are used in such synthesis routes can remain strongly adsorbed on the nanoparticles' surfaces and can then lead to a decrease in catalytic performance. The complete removal of capping agents without altering the surface structures and shapes of the nanoparticles can be challenging, but is sometimes possible using special decontamination procedures [37,38].

In 2012, Carpenter et al. described the solvothermal synthesis of octahedral, cubic, and cubo-octahedral Pt–Ni alloy nanoparticles using N,N-dimethylformamide (DMF), which acts as both a solvent and a reducing agent during synthesis [9]. Unlike other methods that require capping agents such as oleylamine [7], no dedicated surfactants were needed to achieve shape-selective growth, resulting in clean nanoparticle surfaces for catalytic applications. The authors showed that the ORR activity of the alloy nanoparticles was almost 15 times higher than that of a state-of-the-art Pt/C catalyst. Subsequently, Cui et al. used a DMF-based solvothermal approach to synthesize octahedral Pt–Ni nanoparticles that had high ORR activity [12,39].

In 2013, Choi et al. described octahedral Pt–Ni nanoparticles with a specific ORR activity that was 51 times higher than that of a Pt/C catalyst and a record-high mass activity of 3.3 A/mg Pt [40]. The same group optimized catalytic activity toward the ORR by controlling the nanoparticle size and composition for this synthesis, finding the highest mass activity for $Pt_{2.4}Ni$ octahedra with an edge length of 9 nm [41]. The high activity of the nanoparticles was attributed to the presence of very clean surfaces resulting from the use of a new synthesis protocol. After 5 k cycles, the nanoparticles showed a decrease in Pt mass activity by 40%, which is higher than that of Pt/C (32%) [40].

Recently, Park et al. demonstrated a modified growth procedure that can be used to synthesize Pt–Ni octahedra covered by ultrathin Pt shells, which protect Ni from being leached off and enhance the stability of the nanoparticles [42]. The Pt shell octahedra were synthesized by the dropwise injection of a Pt precursor solution into an as-obtained suspension of Pt–Ni octahedra. The authors demonstrated that the catalyst showed a remarkable enhancement in electrocatalytic durability toward the ORR relative to a Pt–Ni catalyst and significantly enhanced chemical stability with less Ni decomposition [42].

In summary, many different routes for the synthesis of octahedral Pt–Ni-based alloy nanoparticles with different sizes, compositions, and properties have now been described. It has been demonstrated that this class of catalysts provides record activity and improved stability.

3. Microstructural investigations

A large number of studies have highlighted the importance of understanding the atomic structures of catalytically active nanoparticles, such as the presence of a Pt-rich skin [6], in order to tune their properties. It is clear that the sizes, shapes, compositions, and local elemental distributions of nanoparticles are essential parameters that determine their catalytic performance [43–46]. For the rational design of new catalysts, it is therefore essential to understand the microstructural evolution of the constituent nanoparticles, both during growth and during degradation.

TEM and scanning TEM (STEM), in combination with energy-dispersive X-ray spectroscopy (EDX) and electron energy-loss spectroscopy (EELS), are among the most widely used atomic-scale characterization techniques. Over the last decade, progress in electron microscopy, resulting in particular from the development of spherical aberration (C_S) correction [47,48], has resulted in an achievable spatial resolution of better than 0.1 nm, in combination with the use of high beam currents for spectroscopic investigations. Substantial progress in analytical electron microscopy has also recently been achieved by the introduction of large-solid-angle silicon drift detectors (SDDs). For instance, the so-called Super-X detector, which makes use of four windowless SDDs that are placed symmetrically around the optical axis close to the sample area, has a much higher X-ray collection efficiency than previous conventional EDX detectors, providing a large total sensor area of 120 mm^2 and a detection solid angle of 0.7 sr [49]. Furthermore, improvements in probe currents obtained using high-brightness field emission gun electron sources in C_S-corrected STEMs has decreased collection times in analytical electron microscopy. Such advances in microstructural analysis have had a very significant impact on materials science in general and on the study of catalyst nanoparticles in particular [50–52].

In addition to traditional *ex situ* TEM/STEM studies of morphological and structural changes that have taken place during electrochemical cycling at different stages of chemical reactions, *in situ* investigations now offer new perspectives. For example, using microelectromechanical systems (MEMS)-based TEM specimen holders it is possible to record the atomic and/or electronic structures of materials, including the evolution of their size and shape, in real time during electrochemical reactions and growth processes at elevated temperature and/or in gas or liquid environments [53–61].

4. Anisotropic growth

4.1. Binary Pt–Ni nanoparticles

In 2013, Cui et al. [12] described inhomogeneous compositional distributions in shaped Pt alloy nanoparticles, in the form of Pt-rich frames and Ni-rich facets. They established that selective etching of Ni-rich {1 1 1} facets during electrochemical cycling had resulted in the formation of concave octahedra, thereby exposing less active facets such as {1 0 0} and {1 1 0} and leading to a significant decrease in activity [12]. In 2014, Gan et al. showed that the atomic-scale growth mechanism of octahedral Pt–Ni nanoparticles results in an inhomogeneous elemental distribution [39]. The latter study is reviewed in the following paragraph.

Pt–Ni alloy nanoparticles were analyzed using high-angle annular dark field (HAADF) STEM and EELS elemental mapping after 4, 8, 16, and 42 h of solvothermal synthesis. After a reaction time of 4 h, most of the nanoparticles exhibited near-spherical shapes with diameters of between 2 and 8 nm, although some

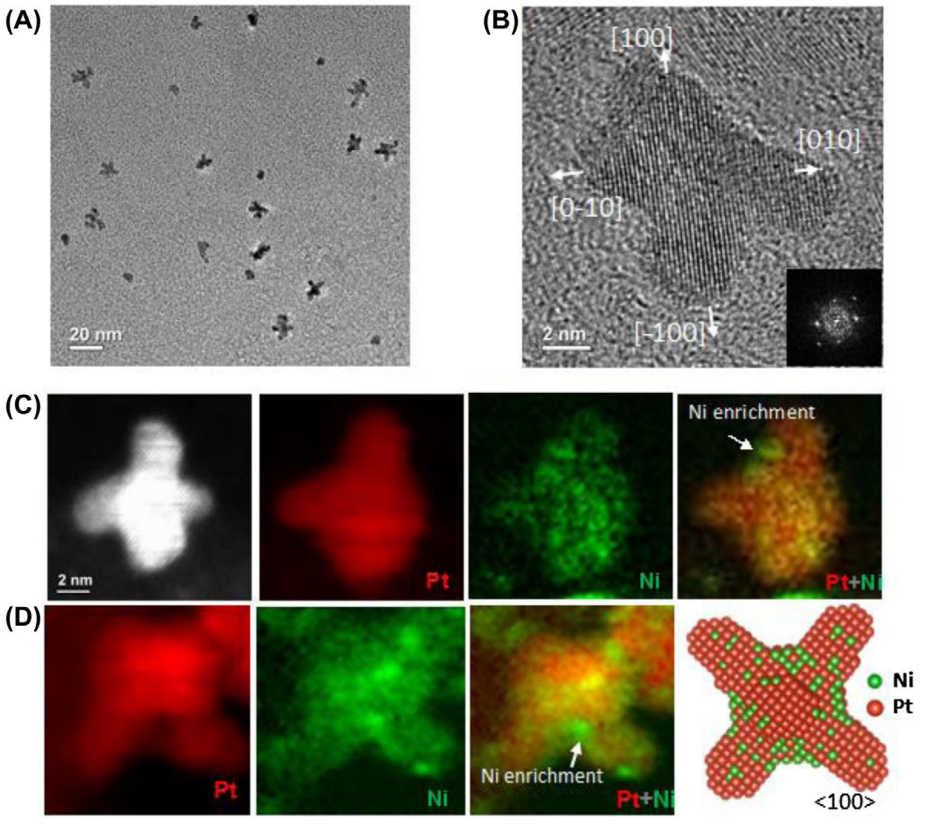

Figure 1. Characterization of Pt–Ni nanoparticles after 8 h of reaction time. (A) Low-magnification TEM image. (B) HRTEM image and corresponding digital diffractogram (Fourier transform) of a nanoparticle that branched along the <1 0 0> directions. (C, D) HAADF STEM images (red) representing Pt and EELS spectrum images recorded using the Ni L-edges (green), indicating that Ni has segregated to the concave surface of Pt–Ni hexapod nanoparticles [39].

nanoparticles had formed branched structures with larger sizes of between 6 and 12 nm. After 8 h, most of the nanoparticles had evolved into hexapod structures with average sizes of approximately 11 nm (Figure 1(A) and (B)).

EDX composition analysis showed that the particles are initially highly Pt-rich, but that their Ni content increases during synthesis. Figure 1(C) and (D) show elemental maps of Ni-rich regions formed on the concave surfaces of previously formed Pt-rich hexapod nanoparticles. After a reaction time of 16 h, a transformation of the hexapod nanoparticles to 'concave octahedra' takes place (Figure 2(A)), which is consistent with accelerated deposition of a Ni-rich phase on the concave surfaces. The schematic diagrams in Figure 2(B) show that, after 8 h, the Pt-rich hexapods have intrinsic {1 1 1} surface steps on their concave surfaces and {1 0 0}/{1 1 0} steps on the sidewalls of their arms. When compared with the terrace sites, Ni adatoms energetically prefer the step sites as a result of their higher coordination number. Deposition of a Ni atom onto a step results in its

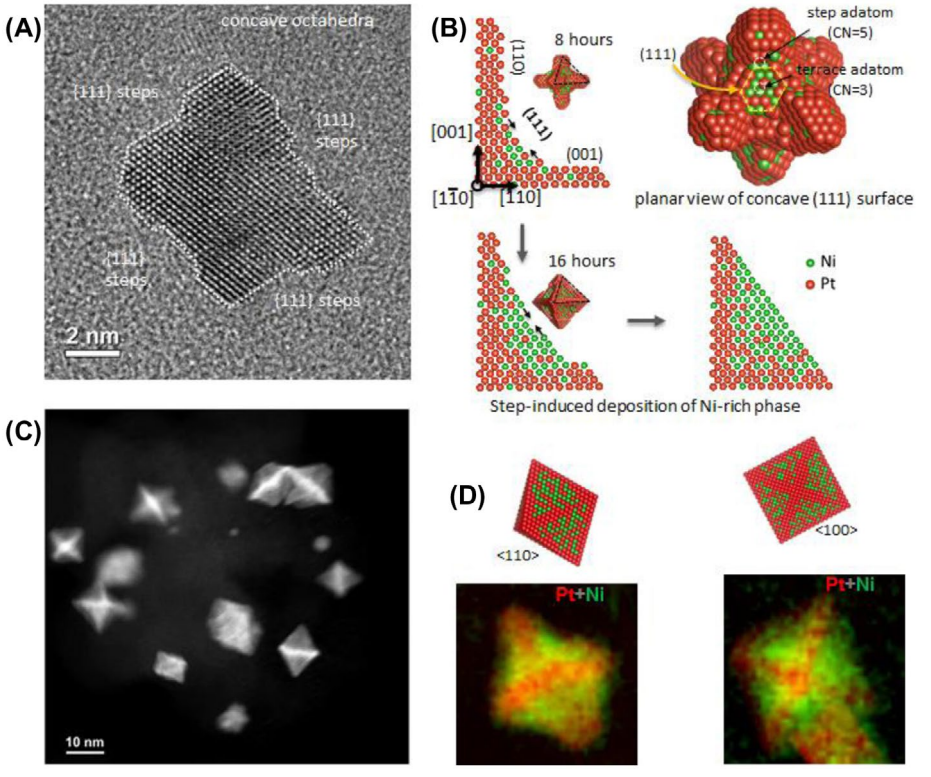

Figure 2. (A) HRTEM image of a 'concave octahedral nanoparticle' studied after growth for 16 h, viewed along a <1 1 0> direction and showing atomic surface steps on concave {1 1 1} facets. (B) Schematic diagrams illustrating delayed anisotropic growth of a Ni-rich phase by the step-induced layer-by-layer deposition of Ni-rich atoms on the concave {1 1 1} surfaces of pre-formed Pt-rich hexapods. (C, D) Characterization of final Pt–Ni nanooctahedra after a reaction time of 42 h. (C) HAADF STEM image. (D) HAADF STEM images (red) mainly representing Pt and EELS spectrum images recorded using the Ni L-edges (green) recorded from octahedral $PtNi_{1.5}$ nanoparticles. The images reveal Pt-rich frames along the edges/corners of the nanoparticles and Ni-enriched facets [39].

advance, leading to continuous, step-induced deposition of primarily Ni atoms. In this context, the sidewalls play an important role by providing initial step sites to induce the layer-by-layer growth of Ni-rich {1 1 1} facets. Taken together, the nanoparticle formation process proceeds spontaneously in a one-pot synthesis, creating highly geometric but compositionally anisotropic nanooctahedra, while allowing the degree of concavity to be controlled simply by altering the reaction time.

Ultimately, the transformation to octahedral Pt–Ni nanoparticles with smooth {1 1 1} surfaces is complete after a reaction time of 42 h (Figure 2(C)). The average Ni composition has then increased to $Pt_{40}Ni_{60}$, although the nanoparticle size has increased only slightly. As the Ni-rich phase reaches the tops of the hexapod arms and flat {1 1 1} surfaces are formed, there are no further step edges available, resulting in the termination of metal deposition and an octahedral shape. In

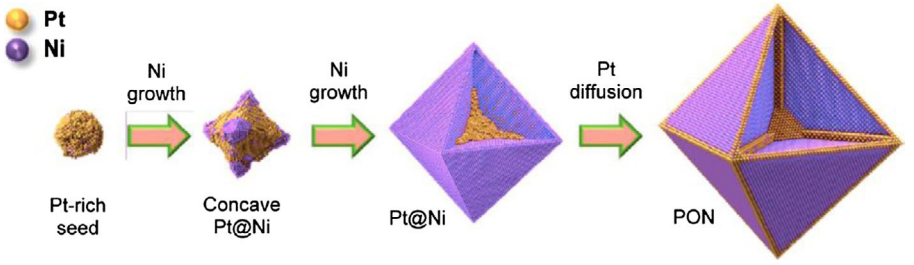

Figure 3. Schematic diagram illustrating the formation of a Ni-rich phase-segregated octahedral nanoparticle (PON), showing the formation of a Pt-rich frame with <1 1 0> edges and <1 0 0> inner axes. Reprinted with permission from Ref. [62]. Copyright 2015 American Chemical Society.

conclusion, the results of Gan et al. reveal an element-specific compositionally anisotropic growth mechanism, with rapid growth of Pt-rich hexapods along <1 0 0> directions preceding the delayed deposition of a Ni-rich phase on concave {1 1 1} sites, which results in the formation of compositionally anisotropic octahedral nanoparticles with Ni-enriched faces (Figure 2(D)) [39].

In 2015, Oh et al. investigated CO-induced phase segregation in octahedral nanoparticles [62], which were, in contrast to the work of Gan et al. [39], distinctly larger and more Ni-rich. They observed geometrically highly symmetrical phase-segregated Pt–Ni nanostructures, comprising Ni octahedra encased by octahedral Pt frameworks with three intersecting perpendicular Pt axes [62]. Small, geometrically poorly defined Pt-rich Pt–Ni alloy nanocrystals were inferred to have formed initially, with a subsequent gradual transformation into slightly concave octahedral nanoparticles (Figure 3). Growth of the Ni phase then followed, resulting in the formation of octahedral core–shell Pt–Ni nanoparticles. Shape control of the Ni-rich octahedral nanoparticles was assisted by the octahedral shapes of the Pt–Ni concave nanocrystal seeds. The protruding ends of the Pt-rich concave nanoparticles continued to form during the nanoparticle growth process by selectively recruiting Pt precursors over Ni precursors. Prolonged heating of the Pt–Ni nanoparticles in the presence of CO finally led to Pt migration from the cores to the surfaces and to the formation of Pt-rich lines along the <1 1 0> edges and the three perpendicular inner axes. The underlying mechanism of anisotropic nanoscale phase segregation is thought to be associated with strain energy minimization.

Although the chemical routes for the nanoparticle synthesis are different, a comparison of the growth mechanisms described by Gan et al. and Oh et al. shows distinct similarities especially at the beginning of the growth [39,62]. In the two studies, growth starts very similarly from Pt-rich seeds, which develop further into concave octahedral structures. The formation of the latter structures is, however, different, as a Pt-rich outer frame with <1 1 0> edges is formed in the case of the Ni-rich nanoparticles investigated by Oh et al. [62]. Further investigation of

Pt alloy nanoparticle structure formation as a function of synthesis and growth conditions is a remaining challenge for further investigations.

4.2. Ternary Pt–Ni–Co nanoparticles

The addition of a ternary element opens up vast possibilities for enhancing ORR performance through compositional tuning. Ternary octahedral Pt–Ni-based nanoparticles, such as Pt–Ni–Fe and Pt–Ni–Cu, which have high activity and promising stability for the ORR, were recently described [63,64]. Based on the high activity and stability of binary Pt–Co catalysts [65–67], ternary Pt–Ni–Co alloy catalysts in particular have recently attracted attention [68,69], with precise control over the composition, size, and phase of the Pt–Ni–Co nanoparticles during synthesis and subsequent treatment identified as being crucial for their electrocatalytic activity and stability. The addition of a third element such as Co introduces an additional degree of freedom that can be used to tune and optimize the d-band center and hence the ORR activity [70]. However, the primary challenge for the synthesis of ternary octahedral nanoparticles is to obtain different compositions while maintaining an octahedral morphology for the nanoparticles.

In 2014, octahedral Pt–Ni–Co/C catalysts with a relatively low Co content ($Pt_{71}Ni_{25}Co_4$) were reported by Huang et al. as being promising and highly efficient catalysts for the ORR [14]. One-pot growth was used to synthesize ternary Pt–Ni–Co octahedra with high activities of up to 2.33 A/mg Pt and higher stability than commercial Pt/C [71].

Aran-Ais et al. presented a growth study of ternary Pt–Ni–Co nanooctahedra via low temperature, surfactant-free solvothermal synthesis [72]. In a 'one-step' approach, they showed that Ni reduction prevails over Co reduction. As a result, STEM and EDX investigations showed that Co was present primarily on the surfaces of the nanoparticles. The authors showed that a 'two-step' synthesis, with Pt and Co reduced simultaneously in the first step of the growth process and Ni added in the second step, led to the formation of octahedral nanocatalysts with both Co and Ni more homogeneously distributed on the {1 1 1} facets.

Recently, Zhao et al. described a one-step synthesis method for the growth of octahedral Pt–Ni–Co ternary catalysts with tunable compositions and fixed shapes [73]. Impressively, the octahedral $PtNi_{0.55}Co_{0.1}$/C nanoparticles showed significantly improved ORR activity when compared with previously reported Pt–Ni–Co alloy octahedra, exhibiting an outstanding mass activity of 2.80 A/mg Pt that was approximately 15 times higher than for Pt/C catalysts.

Another approach that can be used to tune the surface electronic structures of octahedral Pt–Ni nanoparticles was recently proposed by He et al. [74]. They utilized a dealloying process to fabricate an interface between the Pt–Ni nanoparticles and an amorphous nickel boride membrane. The membrane worked as an electron acceptor to tune the surface electronic structure of the Pt–Ni catalyst,

resulting in a 27-fold enhancement in ORR mass activity when compared to commercial Pt/C catalysts.

4.3. Scalable synthesis

Synthesis routes for octahedral nanoparticles are usually batch-based and so are typically limited to a scale of 5–100 mg, i.e. far below industrial scales. By combining the advantages of solid state chemistry and wet synthetic chemistry, Zhang et al. developed a scalable, surfactant-free, cost-effective method to synthesize octahedral Pt–Ni alloy nanoparticles on a C support [75].

LaGrow et al. described the continuous-flow synthesis of Pt alloy nanooctahedra and investigated the effects of precursors on their size and on the elemental distribution within the nanoparticles [76]. They successfully tuned the sizes of monodisperse octahedral Pt–Ni and Pt–Cu alloy nanoparticles between 3 and 16 nm for Pt–Cu and between 4 and 11 nm for Pt–Ni using acetylacetonate or halide precursors of Pt(II), Pt(IV), and Ni(II) or Cu(II). Their approach is fully scalable and can be performed continuously on an industrial scale.

Niu et al. reported the use of a droplet reactor for the continuous and scalable synthesis of octahedral Pt–Ni nanoparticles that showed high ORR performance [77], with control over the sizes and compositions of the nanoparticles. For example, $Pt_{2.4}Ni$ octahedra with an edge length of 9 nm showed a mass activity of 2.67 A/mg Pt, representing an 11-fold improvement over state-of-the-art Pt/C catalysts.

5. Degradation

5.1. Binary Pt–Ni nanoparticles

In 2012, Carpenter et al. used HAADF STEM and EDX to examine Pt–Ni nanoparticle catalysts after rotating disk electrode (RDE) testing and 20 k electrochemical cycling [9]. They noted that the nanoparticles had changed significantly during ORR testing and had developed voids or hollows, presumably as a result of Ni dissolution. While a number of the nanoparticles from the ORR-tested catalyst had acquired voids, other nanoparticles appeared to be unchanged. The nanoparticles that had developed voids retained a high degree of faceting, i.e. the process occurred largely on their {1 1 1} surfaces rather than at their edges. EDX analysis of the hollowed Pt–Ni nanoparticles indicated that they had a lower Ni content than the initial nanoparticles, confirming that void formation had resulted from a loss of Ni.

In 2013, Cui et al. followed the structural degradation of octahedral Pt–Ni nanoparticles by monitoring their catalytic activity along with their compositional and structural evolution [12]. They reported that dealloying under electrochemical conditions resulted in concave octahedral corrosion on {1 1 1} facets. Collapse of the near-surface alloy structure and a loss of active {1 1 1} surfaces on the Ni-rich

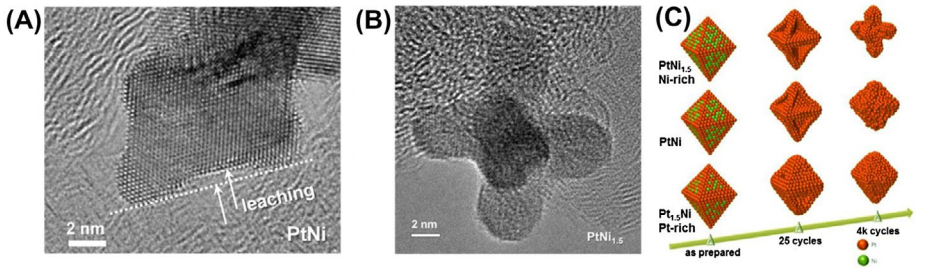

Figure 4. (A, B) HRTEM images of PtNi and $PtNi_{1.5}$ octahedral nanoparticles. (A) Selective leaching after 25 cycles leads to concave shaped facets. (B) Strong selective leaching of the Ni-rich facets after 4 k cycles results in the formation of dendritic hexapod structures. (C) Schematic diagrams of $PtNi_{1.5}$, PtNi and $Pt_{1.5}Ni$ nanoparticle morphologies and surface structures after electrochemical surface activation (25 potential cycles) and electrochemical stability tests (4 k potential cycles), in comparison to as-synthesized nanoparticles [12].

octahedra affected the surface adsorption of oxygen and decreased ORR activity. The results of this study are presented in more detail in the following paragraphs.

Octahedral $Pt_{1.5}Ni$, PtNi, and $PtNi_{1.5}$ nanoparticles that have been prepared using a solvothermal method [10,12] show inhomogeneous elemental distributions with Pt-enriched edges and corners and Ni-rich facets. In order to obtain insight into how the ORR activity of PtNi octahedra correlates with structural, compositional and morphological changes, atomic-scale STEM/EELS studies of the activated catalysts were performed. Figure 4(A) shows results obtained from PtNi nanoparticles after 25 voltammetric potential cycles and provides insight into the transformation of the {1 1 1} facets during electrochemical activation. Only the facet centers show leaching, resulting in a concave curvature. Stability tests for 4 k potential cycles showed a drop in Pt mass activity for the $Pt_{1.5}Ni$, $PtNi_{1.5}$, and PtNi catalysts by 16, 45, and 66%, respectively. This difference in ORR activity is controlled by the (near) surface structure and composition. PtNi shows high initial and activated activity. However, its structural transformation during cycling then affects its activity severely. Microstructural investigations reveal a dramatic morphological degradation for $PtNi_{1.5}$, with the nanooctahedra transforming into hexapod skeletons, on which the catalytically active {1 1 1} facets become lost (Figure 4(B)). Figure 4(C) summarizes the morphological evolution of $Pt_{1.5}Ni$, PtNi, and $PtNi_{1.5}$ nanoparticles. It is noticeable that the Pt-rich $Pt_{1.5}Ni$ nanoparticles undergo the smallest structural transformations during electrochemical processing and largely maintain their octahedral morphology which is also reflected in the smallest drop in Pt mass activity.

5.2. Surface-doped Pt–Ni nanooctahedra

As discussed above, the degradation of Pt–Ni nanooctahedra depends on the local distribution and content of the respective elements. Ni-rich nanooctahedra

lose their shapes through dealloying of Ni-rich facets and can degenerate into Pt-rich hexapod structures. In contrast, catalyst degradation due to dealloying is not as pronounced for Pt-rich nanoparticles, where a loss of shape due to Pt atom surface diffusion is the primary reason for degradation. Surface doping with a ternary metal can then be a highly effective strategy to stabilize the octahedral shapes of the catalyst nanoparticles and to improve their long-term stability during electrochemical cycling.

Huang et al. used an efficient one-pot approach to prepare Pt_3Ni octahedra that had edge lengths of 4.2 nm and were surface-doped with different ternary metals (vanadium, chromium, manganese, iron, cobalt, molybdenum, tungsten, or rhenium) [14]. They showed that, in particular, Mo-doped Pt_3Ni/C has an extraordinary ORR performance, with a high specific activity (10.3 mA/cm^2) and a high mass activity (6.98 A/mg Pt). These record activities provide 81-fold and 73-fold enhancements when compared with a state-of-the-art Pt/C catalyst. The authors also showed that Mo-doped Pt_3Ni/C octahedral catalysts retain their activity after 8 k potential cycles between 0.6 and 1.1 V versus RHE. The activity of the Mo-Pt_3Ni/C catalyst was still as high as 9.7 mA/cm^2 and 6.6 A/mg Pt, showing decreases of only 6.2 and 5.5 % from the initial specific activity and mass activity, respectively. Density functional theory (DFT) calculations suggested that Mo segregates preferentially to the nanoparticle surfaces, where it is most stable on vertex sites. The calculations suggested that Mo stabilizes Ni and Pt atoms against dissolution and may inhibit diffusion through the formation of strong Mo–Pt and Mo–Ni bonds.

Following a similar strategy to that of Huang et al. [14], Beermann et al. described Rh-doped Pt–Ni octahedral nanoparticles that showed improved performance when compared with undoped Pt–Ni octahedral nanoparticles [78]. The authors also showed that surface doping improves the long-term stability of the nanoparticles by maintaining their octahedral shapes with active (1 1 1) facets. In order to provide a reference for the Rh-doped Pt–Ni nanooctahedra, undoped Pt–Ni nanoparticles with average initial compositions of 79 at.% Pt and 21 at.% Ni were studied using HAADF STEM and EDX in their initial states and also after 4 and 8 k cycles (see Figure 5). EDX maps acquired for the initial state and the 4 k state show enrichment of Ni on the facets. After 8 k cycles, the octahedral shape is lost and the nanoparticles become nearly spherical. In addition, a Pt-rich shell is built up around the spherical nanoparticles, preventing the Ni from being leached off. No significant change in alloy composition was found, in contrast to the observation of dealloying in Ni-rich octahedral Pt–Ni nanoparticles [12].

Under the same conditions, Rh-doped Pt–Ni showed much higher stability in shape after 4, 8, and even 30 k cycles. Initially, Rh accumulated on the surfaces of the nanoparticles (Figure 5(D)), in accordance with the results of CO-stripping experiments [76]. EDX quantification yielded an average composition of Pt 69 at.%, Ni 26 at.%, and Rh 5 at.% for the nanoparticles in their initial state. After 4 k cycles, the Rh content dropped to approximately 2 at.%. The octahedral shape was

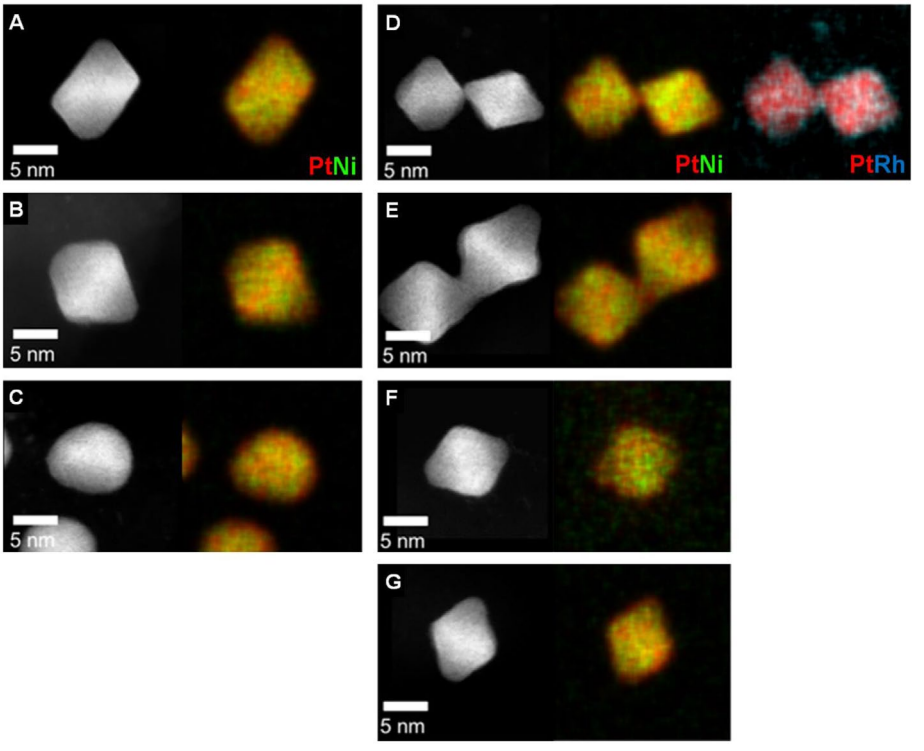

Figure 5. HAADF STEM images and EDX maps of (A–C) Pt–Ni and (D–G) Rh-doped Pt–Ni nanoparticles. (A, D) show the initial state, while (B, E) were acquired after 4 k, (C, F) after 8 k and (G) after 30 k cycles. Although the Pt–Ni nanoparticles become spherical after 4 k cycles, the Rh-doped Pt–Ni nanoparticles retain their octahedral shapes even after 30 k cycles. Reprinted with permission from Ref. [78]. Copyright 2016 American Chemical Society.

retained even after 30 k cycles, with an outermost Pt-enriched shell. It is plausible that shape losses in binary Pt–Ni nanoparticles result primarily from Pt atom diffusion during dynamic potential cycling, as demonstrated by the formation of a Pt-rich shell around the Pt–Ni nanoparticles after 4 k cycles. It was also demonstrated that Rh effectively suppresses the diffusion of Pt atoms, maintaining the octahedral shapes of the nanoparticle catalysts.

Recently, Cao and Mueller provided theoretical insight into the effects of Mo surface doping on the stability of octahedral Pt–Ni nanoparticles [79]. Using *ab initio* calculations, they showed that surface doping has a twofold influence on the shape stability of octahedral nanoparticles. As mentioned above, there two primary mechanisms are responsible for shape loss and degradation: Ni dissolution from Ni-rich {1 1 1} facets (Figure 5) [12] and Pt surface migration (Figure 5) [78]. Cao and Mueller demonstrated that Mo doping protects against Ni dissolution by significantly reducing the equilibrium Ni composition in the surface layer of the octahedral Pt_3Ni nanoparticles under oxidizing conditions, especially on vertex and edge sites [79]. As a result, there is a reduced driving force for Ni atoms to

migrate to the vertex and edge sites, which are more vulnerable to dissolution. They also showed that Mo doping increases Pt and Ni vacancy formation energies on vertex sites, as well as for other poorly coordinated atoms such as those at step edges. In this way, Mo stabilizes surface atoms and prevents Pt (or Ni) surface migration. The combination of a reduction in equilibrium surface Ni composition and the stabilization of sites with low coordination provides an explanation for how Mo surface doping effectively stabilizes the shapes and compositions of octahedral Pt_3Ni nanoparticles.

6. Present and future challenges for advanced electron microscopy of octahedral Pt–Ni nanoparticles

6.1. In situ *electron microscopy*

The use of state-of-the-art *in situ* techniques, such as those based on MEMS-based heating, gas and liquid cell TEM specimen holders, has greatly expanded the capabilities of high spatial resolution experiments in the electron microscope. In this section, we briefly summarize recent *in situ* investigations on octahedral Pt alloy nanoparticles and discuss possible future trends in technique and instrumentation development that are relevant for studies of the growth of nanoparticles in liquid environments.

The influence of Pt atom surface diffusion on the shapes of octahedral Pt–Ni nanoparticles during *in situ* annealing was studied by Gan et al. using TEM and STEM in a MEMS-based heating system [80]. The nanoparticles, which were initially slightly concave in shape, became spherical above 600 °C due to surface diffusion of Pt atoms from their corners/edges to their facets. However, annealing to 500 °C resulted in the diffusion of Pt surface atoms from the corners/edges onto the concave Ni-rich {1 1 1} surfaces, leading to perfectly flat Pt-rich {1 1 1} surfaces with Ni-rich sub-surface layers. Thermal annealing of Ni-rich octahedral nanoparticles can therefore be used to create Pt-rich {1 1 1} surfaces with Ni-rich sub-surface layers, which are expected to be more catalytically active and stable. Pan et al. recently investigated the dynamics of thermally induced compositional redistribution within octahedral PtNi nanoparticles *in situ* in an environmental TEM using a tungsten heating wire sample holder and observed a change in Ni content on their surfaces [81]. In addition to the observations made by Gan et al. they observed dislocation motion within PtNi octahedra during heating. The thermally treated PtNi catalysts showed a significant ORR activity of 1.4 A/mgPt. This study demonstrated the importance of post-synthesis thermal treatment on the optimization of the Pt and Ni atomic distribution.

The direct *in situ* growth of faceted Pt–Ni alloy nanoparticles in the electron microscope would be highly desirable. Recent developments in MEMS chip-based closed liquid cells have paved the way toward such studies. Here, we briefly discuss recent experiments that have been performed using liquid cells to study the growth

of faceted nanoparticles. Such electron microscopy studies in liquid environments are particularly challenging, as a result of the influence of the electron beam on the reactions, the low signal-to-noise ratio of the recorded images and the speed of conventional digital cameras. The recent development of new fast direct detection cameras has significantly improved the sensitivity and temporal resolution of images recorded during *in situ* experiments in the electron microscope. Liao et al. imaged the growth of faceted Pt nanocubes in a liquid cell with high spatial and temporal resolution using a MEMS chip-based liquid cell specimen holder and a fast direct detection camera [82]. They showed that the growth rates of all of the low-index facets are initially similar, until the {1 0 0} facets stop growing at a certain nanoparticle size. They used calculations to determine that the mobility of the ligands that they used is lowest on {1 0 0} facets, thereby preventing Pt atoms from landing on the {1 0 0} facets. Similar growth reactions, involving the growth of spherical nuclei into faceted particles, were reported by De Clercq et al. using *in situ* TEM [83]. This experiment was performed in a liquid encapsulated between two graphene oxide sheets. This technique, which was initially introduced by Yuk et al. in 2012 using a graphene-encapsulated liquid cell, allows atomic-resolution imaging while sustaining the most realistic liquid conditions achievable under minimum background scattering conditions [84].

6.2. Toward atomic-scale three-dimensional nanoparticle structures

In the preceding paragraphs, we have reviewed the current state of research on the growth and degradation of octahedral Pt alloy nanoparticle catalysts and have shown that atomic-scale analytical electron microscopy is an essential characterization tool. We have stated that the investigation of the three-dimensional atomic structures of octahedral catalysts, such as the formation of Pt atomic layer skins, is essential in order to understand their electrocatalytic performance. However, true atomic-scale three-dimensional structural information has not yet been obtained experimentally for octahedral PtNi nanoparticles. Here, we discuss prospects for applying electron microscopy to obtain quantitative structural and compositional atomic-scale information about octahedral nanoparticle catalysts in all three dimensions.

As previously mentioned, EDX mapping has now become routinely possible in more reasonable timescales, providing a significant impact for nanoparticles, where such a small mass of samples requires the new generation large-solid-angle SSD detectors in order to achieve meaningful count rates. For more than 40 years, EDX quantification has been performed primarily using the Cliff–Lorimer approach, which relates the composition of the constitutive elements in a thin specimen to the measured characteristic X-ray intensities [85]. A major limitation of this approach is that X-ray absorption correction requires additional measurement of the sample thickness and the requirement of several alloy standards with carefully known composition. A more advanced approach, which has X-ray

absorption 'built-in' because it all provides information about the mass-thickness of the sample, is the so-called ζ-factor method [86]. This method uses pure element (instead of multi-element) standards which are much more readily available. More recently still, the partial cross section method allows X-ray counts to be quantified on an absolute scale, in order to provide the number of atoms in the sample [87]. This method has been applied successfully to the analysis of PtCo nanoparticle catalysts, showing Co depletion at the surfaces of Pt/Co acid-leached nanoparticles and demonstrating clear benefits for the quantitative characterization of local composition for multicomponent nanoparticle catalysts [88].

In addition to improvements in EDX detector efficiency, advanced EELS offers new prospects. By making use of a modern EELS spectrometer with high energy dispersion, a highly monochromated electron beam and an ultra-bright cold field emission gun, Krivanek et al. recently demonstrated vibrational spectroscopy in the electron microscope [89]. The authors also demonstrated 'aloof' beam analysis with the electron beam positioned outside sample. This approach largely avoids radiation damage for electron-beam-sensitive samples and may therefore provide a useful method to avoid radiation damage in small nanoparticles or clusters, especially in the presence of organic ligands.

Electron beam damage and the reorientation of nanoparticles under the electron beam are strong constraints when imaging nanoparticle catalysts, especially during multiple image acquisition for electron tomography. As ADF STEM is highly sensitive to the number of atoms an atomic column, ADF STEM atom counting is potentially of great relevance for the determination of the three-dimensional structures of nanoparticles and clusters [90]. A three-dimensional reconstruction of a crystalline nanoparticle at atomic resolution can in principle be attained by combining aberration-corrected STEM atom counting with discrete tomography. Unlike for conventional electron tomography, only two images of the nanoparticle may be sufficient for reconstruction. This method is potentially applicable for the atomic characterization of complex single-element nanoparticles, as well as complex nanostructures. With regard to avoiding electron beam damage, De Backer et al. analyzed the dose-limited reliability of quantitative ADF STEM for atom-counting and explored the minimum electron dose that is necessary for single-atom counting precision. They showed that careful compensation for varying contrast of the carbon support is necessary to avoid atom-counting errors and that care must be taken in the interpretation of column intensities for slightly tilted nanoparticles [91].

Most of the methods for three-dimensional analysis that have been described so far have been focused on the investigation of single-element nanostructures and nanoparticles. Goris et al. reported the three-dimensional structure of a binary Au/Ag nanorod [92]. They distinguished Ag from Au atoms by combining compressive-sensing-based HAADF STEM tomography with statistical parameter estimation methods. Using five high-resolution Z-contrast HAADF-STEM images recorded along different zone axes, a full three-dimensional

reconstruction of the positions and types of the constituent atoms was possible, enabling the investigation of the core–shell interface with atomic sensitivity. The combination of discrete tomography with atom counting by ADF STEM and EDX, for instance by calculating EDX partial cross sections as recently presented by MacArthur et al. [87,88], is therefore a promising route for obtaining atomic-scale three-dimensional compositional and structural information about catalyst nanoparticles. However, such experiments are currently very labor-intensive and would benefit significantly from the automation of future electron microscopes, as well as from new approaches for data handling.

In addition to ADF STEM, high-resolution aberration-corrected TEM combined with dedicated numerical evaluation procedures allows the three-dimensional shapes of crystals to be determined from single high-resolution images, as recently demonstrated for an MgO crystal viewed along [0 0 1] [93]. The sensitivity of the reconstruction procedure is not only sufficient to reveal the surface morphology of the crystal with atomic spatial resolution, but also to detect the presence of adsorbed impurity atoms. Such a single-image approach may offer possibilities to detect changes in the surface morphologies of individual nanoparticles during *in situ* chemical reactions.

A visionary three-dimensional imaging approach was investigated theoretically by Ishikawa et al. They examined the prospects of using a confocal STEM approach for atom-by-atom imaging [94], demonstrating the feasibility to image surface atomic structures, three-dimensional atomistic morphologies and the depth locations of single dopant atoms using large-angle illumination STEM in a single crystallographic orientation. This technique would also allow depth-sensitive spectroscopy to be performed. However, it would depend strongly on the further development of higher order geometric and chromatic aberration correctors, as a large illumination angle of more than 60 mrad is required.

7. Conclusions

As a result of the unusual electronic structure manifested by its d-band center position, the Pt_3Ni (1 1 1) surface has a 90-fold higher activity for the ORR than current state-of-the-art Pt/C catalysts. (1 1 1)-faceted octahedral Pt–Ni alloy nanoparticles have therefore been considered to be 'dream electrocatalysts', with large efforts dedicated to their synthesis, electrochemical investigation, and microstructural investigation. Different synthesis routes for octahedral or truncated octahedral nanoparticles have been established. Special capping agents are often used to selectively control the growth rates of individual facets. However, they can also decrease the catalytic performance of the nanoparticles, as they remain adsorbed on the nanoparticle surfaces. Alternative surfactant-free DMF-based solvothermal synthesis routes have been developed.

In this paper, we have reviewed recent research on the application of advanced TEM techniques to the study of the growth, degradation, and stability of Pt–Ni-based nanoparticles. Microstructural studies of nanoparticles at different stages of synthesis

reveal element-specific anisotropic growth, starting with a Pt-rich nucleus that branches along the <1 0 0> directions and forms a concave octahedron structure. Subsequently, Ni fills the {1 1 1} facets, creating a highly compositionally anisotropic structure. Depending on the composition and annealing conditions, a Pt-rich frame with <1 1 0> edges can also be created. Such an anisotropic structure has a strong influence on the degradation of the nanoparticles during electrochemical cycling.

The degradation of octahedral nanoparticles that have initial compositions between $Pt_{1.5}Ni$ and $PtNi_{1.5}$ during electrochemical cycling takes place due to dealloying and a loss of octahedral shape. Octahedral nanoparticles are leached preferentially at their Ni-rich facet centers, evolving into concave octahedra or even, for initially Ni-rich nanoparticles, into hexapod skeletons. As a consequence of the loss of their highly active {1 1 1} facets, their electrochemical performance then drops significantly. In contrast, Pt-rich octahedra do not suffer from pronounced Ni dealloying. Instead, Pt surface diffusion has been identified as the primary reason for degradation due to shape loss, i.e. due to a transformation to spherical nanoparticles.

Surface doping with Mo or Rh has been introduced as an effective strategy to prevent Pt surface diffusion and to stabilize the octahedral shapes of nanoparticles, even during long-term cycling.

Intense recent research into the synthesis, catalytic properties, structure formation and degradation of octahedral Pt–Ni nanoparticle catalysts for the ORR has resulted in highly advanced and structurally complex catalyst nanoparticles with record-breaking activity and highly improved stability.

Future developments in instrumentation and technique in electron microscopy may offer prospects for real-time quantitative studies of nanoparticle synthesis, growth and reactions in realistic environments with atomic spatial resolution in all three dimensions.

Acknowledgments

We are grateful to Peter Strasser, Lin Gan, Chunhua Cui, and Meital Shviro for ongoing collaborations and valuable discussions and Katherine E. MacArthur for proofreading. We thank the Deutsche Forschungsgemeinschaft (DFG) for financial support. Furthermore, this work has received funding from the European Union's Horizon 2020 research and innovation programme.

Disclosure statement

No potential conflict of interest was reported by the authors.

Funding

This work was supported by the Deutsche Forschungsgemeinschaft (DFG) [grant number HE 7192/1–1]; the European Union's Horizon 2020 research and innovation programme [grant number 686053].

References

[1] J.K. Nørskov, J. Rossmeisl, A. Logadottir, L. Lindqvist, J.R. Kitchin, T. Bligaard and H. Jónsson, J. Phys. Chem. B 108 (2004) p.17886.
[2] O.T. Holton and J.W. Stevenson, Platinum Met. Rev. 57 (2013) p.259.
[3] S. Mukerjee, S. Srinivasan, M.P. Soriaga and J. McBreen, J. Electrochem. Soc. 142 (1995) p.1409.
[4] T. Toda, H. Igarashi, H. Uchida and M. Watanabe, J. Electrochem. Soc. 146 (1999) p.3750.
[5] C. Wang, M. Chi, G. Wang, D. van der Vliet, D. Li, K. More, H.-H. Wang, J.A. Schlueter, N.M. Markovic and V.R. Stamenkovic, Adv. Funct. Mater. 21 (2011) p.147.
[6] V.R. Stamenkovic, B. Fowler, B.S. Mun, G. Wang, P.N. Ross, C.A. Lucas and N.M. Markovic, Science 315 (2007) p.493.
[7] J. Zhang, H. Yang, J. Fang and S. Zou, Nano Lett. 10 (2010) p.638.
[8] J. Wu, J. Zhang, Z. Peng, S. Yang, F.T. Wagner and H. Yang, J. Am. Chem. Soc. 132 (2010) p.4984.
[9] M.K. Carpenter, T.E. Moylan, R.S. Kukreja, M.H. Atwan and M.M. Tessema, J. Am. Chem. Soc. 134 (2012) p.8535.
[10] C. Cui, L. Gan, H.-H. Li, S.-H. Yu, M. Heggen and P. Strasser, Nano Lett. 12 (2012) p.5885.
[11] S.-I. Choi, S. Xie, M. Shao, J.H. Odell, N. Lu, H.-C. Peng, L. Protsailo, S. Guerrero, J. Park, X. Xia, J. Wang, M.J. Kim and Y. Xia, Nano Lett. 13 (2013) p.3420.
[12] C. Cui, L. Gan, M. Heggen, S. Rudi and P. Strasser, Nat. Mater. 12 (2013) p.765.
[13] C. Zhang, S.Y. Hwang, A. Trout and Z. Peng, J. Am. Chem. Soc. 136 (2014) p.7805.
[14] X. Huang, Z. Zhao, L. Cao, Y. Chen, E. Zhu, Z. Lin, M. Li, A. Yan, A. Zettl, Y.M. Wang, X. Duan, T. Mueller and Y. Huang, Science 348 (2015) p.1230.
[15] T. Toda, H. Igarashi, H. Uchida and M.J. Watanabe, Electrochem. Soc. 146 (1999) p.3750.
[16] S. Mukerjee and S.J. Srinivasan, Electroanal. Chem. 357 (1993) p.201.
[17] F. Hasché, M. Oezaslan and P. Strasser, ChemCatChem 3 (2011) p.1805.
[18] J. Park, L. Zhang, S.I. Choi, L.T. Roling, N. Lu, J.A. Herron, S. Xie, J. Wang, M.J. Kim, M. Mavrikakis and Y. Xia, ACS Nano 9 (2015) p.2635.
[19] J. Park, M. Vara and Y. Xia, Catal. Today 280 (2017) p. 266. doi:http://dx.doi.org/10.1016/j.cattod.2016.06.045.
[20] S. Prabhudev, M. Bugnet, C. Bock and G.A. Botton, ACS Nano 7 (2013) p.6103.
[21] P. Strasser, S. Koh, T. Anniyev, J. Greeley, K. More, C. Yu, Z. Liu, S. Kaya, D. Nordlund, H. Ogasawara, M.F. Toney and A. Nilsson, Nat. Chem. 2 (2010) p.454.
[22] V. Stamenkovic, B.S. Mun, K.J.J. Mayrhofer, P.N. Ross, N.M. Markovic, J. Rossmeisl, J. Greeley and J.K. Nørskov, Angew. Chem. Int. Ed. 45 (2006) p.2897.
[23] I.E.L. Stephens, A.S. Bondarenko, F.J. Perez-Alonso, F. Calle-Vallejo, L. Bech, T.P. Johansson, A.K. Jepsen, R. Frydendal, B.P. Knudsen, J. Rossmeisl and I.J. Chorkendorff, Am. Chem. Soc. 133 (2011) p.5485.
[24] V. Stamenkovic, B.S. Mun, K.J.J. Mayrhofer, P.N. Ross, N.M. Markovic, J. Rossmeisl, J. Greeley and J.K. Nørskov, Angew. Chem. 45 (2006) p.2897.
[25] V. Stamenkovic, B.S. Mun, K.J.J. Mayrhofer, P.N. Ross and N.M. Markovic, J. Am. Chem. Soc. 128 (2006) p.8813.
[26] C. Wang, M. Chi, D. Li, D. Strmcnik, D. van der Vliet, G. Wang, V. Komanicky, K.C. Chang, A.P. Paulikas, D. Tripkovic, J. Pearson, K.L. More, N.M. Markovic and V.R. Stamenkovic, J.A.C.S. 133 (2011) p.14396.
[27] H.A. Gasteiger and N.M. Marković, Science 324 (2009) p.48.
[28] J.B. Wu, A. Gross and H. Yang, Nano Lett. 11 (2011) p.798.
[29] C. Cui, L. Gan, H.H. Li, S.H. Yu, M. Heggen and P. Strasser, Nano Lett. 12 (2012) p.5885.
[30] Y.E. Wu, S.F. Cai, D.S. Wang, W. He and Y.D. Li, J. Am. Chem. Soc. 134 (2012) p.8975.

[31] N.S. Porter, H. Wu, Z. Quan and J. Fang, J. Accounts Chem. Res. 46 (2013) p.1867.
[32] S.W. Chou, Y.R. Lai, Y.Y. Yang, C.Y. Tang, M. Hayashi, H.-C. Chen, H.-L. Chen and P.-T. Chou, J. Catal. 309 (2014) p.343.
[33] J. Wu, J. Zhang, Z. Peng, S. Yang, F.T. Wagner and H. Yang, J. Am. Chem. Soc. 132 (2010) p.4984.
[34] C. Li, T. Wang, W. Chu, P. Wu and D.G. Tong, Nanoscale 8 (2016) p.7043.
[35] M. Shviro, S. Polani and D. Zitoun, Nanoscale 7 (2015) p.13521.
[36] M. Zhou, H. Wang, M. Vara, Z.D. Hood, M. Luo, T.H. Yang, S. Bao, M. Chi, P. Xiao, Y. Zhang and Y. Xia, J. Am. Chem. Soc. 138 (2016) p.12263.
[37] R.M. Arán-Ais, F.J. Vidal-Iglesias, J. Solla-Gullón, E. Herrero and J.M. Feliu, Electroanalysis 27 (2015) p.945.
[38] R.M. Arán-Ais, J. Solla-Gullón, M. Gocyla, M. Heggen, R.E. Dunin-Borkowski, P. Strasser, E. Herrero and J.M. Feliu, Nano Energy 27 (2016) p.390.
[39] L. Gan, C. Cui, M. Heggen, F. Dionigi, S. Rudi and P. Strasser, Science 346 (2014) p.1502.
[40] S.-I. Choi, S. Xie, M. Shao, J.H. Odell, N. Lu, H.-C. Peng, L. Protsailo, S. Guerrero, J. Park, X. Xia, J. Wang, M.J. Kim and Y. Xia, Nano Lett. 13 (2013) p.3420.
[41] S.-I. Choi, S. Xie, M. Shao, N. Lu, S. Guerrero, J.H. Odell, J. Park, J. Wang, M.J. Kim and Y. Xia, ChemSusChem 7 (2014) p.1476.
[42] J. Park, J. Liu, H.C. Peng, L. Figueroa-Cosme, S. Miao, S.-I. Choi, S. Bao, X. Yang and Y. Xia, ChemSusChem 9 (2016) p.2209.
[43] J. Solla-Gullón, F.J. Vidal-Iglesias and J.M. Feliu, Annu. Rep. Prog. Chem. Sect. C 107 (2011) p.263.
[44] M.T.M. Koper, Nanoscale 3 (2011) p.2054.
[45] M. Shao, A. Peles and K. Shoemaker, Nano Lett. 11 (2011) p.3714.
[46] F.J. Perez-Alonso, D.N. McCarthy, A. Nierhoff, P. Hernandez-Fernandez, C. Strebel, I.E.L. Stephens, J.H. Nielsen and I. Chorkendorff, Angew. Chem. Int. Ed. 51 (2012) p.4641.
[47] C.L. Jia, M. Lentzen and K. Urban, Science 299 (2003) p.870.
[48] M. Lentzen, Microsc. Microanal. 12 (2006) p.191.
[49] L.J. Allen, A.J. D'Alfonso, B. Freitag and D.O. Klenov, MRS Bull. 37 (2012) p.47.
[50] K.W. Urban, Science 321 (2008) p.506.
[51] D.A. Muller, T. Sorsch, S. Moccio, F.H. Baumann, K. Evans-Lutterodt and G. Timp, Nature 399 (1999) p.758.
[52] C. Kiely, Nat. Mat. 9 (2010) p.296.
[53] S. Giorgio, S.S. Joao, S. Nitsche, D. Chaudanson, G. Sitja and C.R. Henry, Ultramicroscopy 106 (2006) p.503.
[54] J.F. Creemer, S. Helveg, G.H. Hoveling, S. Ullmann, A.M. Molenbroek, P.M. Sarro and H.W. Zandbergen, Ultramicroscopy 108 (2008) p.993.
[55] S.B. Vendelbo, C.F. Elkjær, H. Falsig, I. Puspitasari, P. Dona, L. Mele, B. Morana, B.J. Nelissen, R. van Rijn, J.F. Creemer, P.J. Kooyman and S. Helveg, Nat. Mater. 13 (2014) p.884.
[56] F.M. Ross, Science 350 (2015) p.1490.
[57] N. Hodnik, G. Dehm and K.J.J. Mayrhofer, Acc. Chem. Res. 49 (2016) p.2015.
[58] F. Tao and P.A. Crozier, Chem. Rev. 116 (2016) p.3487.
[59] Y. Jiang, H. Li, Z. Wu, W. Ye, Y. Wang, C. Sun and Z. Zhang, Angew. Chem. 128 (2016) p.12615.
[60] R. Farra, A. Rinaldi, M. Greiner, J. Cao, R. Schlögl and M.G. Willinger, Microsc. Microanal. 22 (2016) p.736.
[61] X. Huang, T. Jones, H. Fan and M.G. Willinger, Adv. Mater. Interfaces (2016) p.1600751doi: http://dx.doi.org/10.1002/admi.201600751.

[62] A. Oh, H. Baik, D.S. Choi, J.Y. Cheon, B. Kim, H. Kim, S.J. Kwon, S.H. Joo, Y. Jung and K. Lee, ACS Nano 9 (2015) p.2856.
[63] Y. Li, F. Quan, L. Chen, W. Zhang, H. Yu and C. Chen, RSC Adv. 4 (2014) p.1895.
[64] C. Zhang, W. Sandorf and Z. Peng, ACS Catal. 5 (2015) p.2296.
[65] S. Guo, D. Li, H. Zhu, S. Zhang, N.M. Markovic, V.R. Stamenkovic and S. Sun, Angew. Chem. Int. Ed. 52 (2013) p.3465.
[66] C. Wang, G. Wang, D. van der Vliet, K.C. Chang, N.M. Markovic and V.R. Stamenkovic, Phys. Chem. Chem. Phys. 12 (2010) p.6933.
[67] D. Wang, H.L. Xin, R. Hovden, H. Wang, Y. Yu, D.A. Muller, F.J. Disalvo and H.D. Abruña, Nat. Mater. 12 (2013) p.81.
[68] B.N. Wanjala, R. Loukrakpam, J. Luo, P.N. Njoki, D. Mott, C.J. Zhong, M. Shao, L. Protsailo and T.J. Kawamura, Phys. Chem. 114 (2010) p.17580.
[69] B.N. Wanjala, B. Fang, R. Loukrakpam, Y. Chen, M. Engelhard, J. Luo, J. Yin, L. Yang, S. Shan and C.J. Zhong, ACS Catal. 2 (2012) p.795.
[70] C. Wang, D. Li, M. Chi, J. Pearson, R.B. Rankin, J. Greeley, Z. Duan, G. Wang, D. van der Vliet, K.L. More, N.M. Markovic and V.R. Stamenkovic, J. Phys. Chem. Lett. 3 (2012) p.1668.
[71] X. Huang, Z. Zhao, Y. Chen, E. Zhu, M. Li, X. Duan and Y. Huang, Energy Environ. Sci. 7 (2014) p.2957.
[72] R.M. Arán-Ais, F. Dionigi, T. Merzdorf, M. Gocyla, M. Heggen, R.E. Dunin-Borkowski, M. Gliech, J. Solla-Gullón, E. Herrero, J.M. Feliu and P. Strasser, Nano Lett. 15 (2015) p.7473.
[73] Z. Zhao, M. Feng, J. Zhou, Z. Liu, M. Li, Z. Fan, O. Tsen, J. Miao, X. Duan and Y. Huang, Chem. Commun. 52 (2016) p.11215.
[74] D. He, L. Zhang, D. He, G. Zhou, Y. Lin, Z. Deng, X. Hong, Y. Wu, C. Chen and Y. Li, Nat. Comm. 7 (2016) p.12362.
[75] C. Zhang, S.Y. Hwang, A. Trout and Z. Peng, J. Am. Chem. Soc. 136 (2014) p.7805.
[76] A.P. LaGrow, K. Rahbek Knudsen, N.M. AlYami, D.H. Anjum and O.M. Bakr, Chem. Mater. 27 (2015) p.4134.
[77] G. Niu, M. Zhou, X. Yang, J. Park, N. Lu, J. Wang, M.J. Kim, L. Wang and Y. Xia, Nano Lett. 16 (2016) p.3850.
[78] V. Beermann, M. Gocyla, E. Willinger, S. Rudi, M. Heggen, R.E. Dunin-Borkowski, M.-G. Willinger and P. Strasser, Nano Lett. 16 (2016) p. 1719. doi:http://dx.doi.org/10.1021/acs.nanolett.5b04636.
[79] L. Cao and T. Mueller, Nano Lett. 16 (2016) p.7748.
[80] L. Gan, M. Heggen, C.H. Cui and P. Strasser, ACS Catal. 6 (2016) p.692.
[81] Y.T. Pan, J. Wu, X. Yin and H. Yang, AIChE J. 62 (2016) p.399.
[82] H.-G. Liao, D. Zherebetskyy, H. Xin, C. Czarnik, P. Ercius, H. Elmlund, M. Pan, L.-W. Wang and H. Zheng, Science 345 (2014) p.916.
[83] A. De Clercq, W. Dachraoui, O. Margeat, K. Pelzer, C.R. Henry and S. Giorgio, J. Phys. Chem. Lett. 5 (2014) p.2126.
[84] J.M. Yuk, J. Park, P. Ercius, K. Kim, D.J. Hellebusch, M.F. Crommie, J.Y. Lee, A. Zettl and A.P. Alivisatos, Science 336 (2012) p.61.
[85] G. Cliff and G.W. Lorimer, J. Microsc. 103 (1975) p.203.
[86] M. Watanabe and D.B. Williams, J. Microsc. 221 (2006) p.89.
[87] K.E. MacArthur, T.J.A. Slater, S.J. Haigh, D. Ozkaya, P.D. Nellist and S. Lozano-Perez, Microsc. Microanal. 22 (2016) p.71.
[88] K.E. MacArthur, T.J.A. Slater, S.J. Haigh, D. Ozkaya, P.D. Nellist and S. Lozano-Perez, Mater. Sci. Technol. 32 (2016) p.248.

[89] O.L. Krivanek, T.C. Lovejoy, N. Dellby, T. Aoki, R.W. Carpenter, P. Rez, E. Soignard, J. Zhu, P.E. Batson, M.J. Lagos, R.F. Egerton and P.A. Crozier, Nature 514 (2014) p.209.
[90] S. Bals, S. Van Aert, C.P. Romero, K. Lauwaet, M.J. Van Bael, B. Schoeters, B. Partoens, E. Yücelen, P. Lievens, G. Van Tendeloo, Nat. Commun. 3 (2012) p. 897.
[91] A. De Backer, G.T. Martinez, K.E. MacArthur, L. Jones, A. Béché, P.D. Nellist and S. Van Aert, Ultramicroscopy 151 (2015) p.56.
[92] B. Goris, A. De Backer, S. Van Aert, S. Gómez-Graña, L.M. Liz-Marzán, G. Van Tendeloo and S. Bals, Nano Lett. 13 (2013) p.4263.
[93] C.L. Jia, S.-B. Mi, J. Barthel, D. Wang, R.E. Dunin-Borkowski, K.W. Urban and A. Thust, Nat. Mater. 13 (2014) p.1044.
[94] R. Ishikawa, A.R. Lupini, Y. Hinuma and S.J. Pennycook, Ultramicroscopy 151 (2015) p.122.